

# Self-Powered Si/CdS Flexible Photodetector with Broadband Response from 325 to 1550 nm Based on Pyro-phototronic Effect: An Approach for Photosensing below Bandgap Energy

Yejing Dai, Xingfu Wang, Wenbo Peng, Cheng Xu, Changsheng Wu, Kai Dong, Ruiyuan Liu, and Zhong Lin Wang\*

Cadmium sulfide (CdS) has received widespread attention as the building block of optoelectronic devices due to its extraordinary optoelectronic properties, low work function, and excellent thermal and chemical stability. Here, a self-powered flexible photodetector (PD) based on p-Si/n-CdS nanowires heterostructure is fabricated. By introducing the pyro-phototronic effect derived from wurtzite structured CdS, the self-powered PD shows a broadband response range, even beyond the bandgap limitation, from UV (325 nm) to near infrared (1550 nm) under zero bias with fast response speed. The light-induced pyroelectric potential is utilized to modulate the optoelectronic processes and thus improve the photoresponse performance. Lasers with different wavelengths have different effects on the self-powered PDs and corresponding working mechanisms are carefully investigated. Upon 325 nm laser illumination, the rise time and fall time of the self-powered PD are 245 and 277  $\mu$ s, respectively, which are faster than those of most previously reported CdS-based nanostructure PDs. Meanwhile, the photoresponsivity  $R$  and specific detectivity  $D^*$  regarding to the relative peak-to-peak current are both enhanced by 67.8 times, compared with those only based on the photovoltaic effect-induced photocurrent. The self-powered flexible PD with fast speed, stable, and broadband response is expected to have extensive applications in various environments.

including light emitting diodes,<sup>[1,2]</sup> photodetectors (PDs),<sup>[3–7]</sup> solar cells,<sup>[8–10]</sup> optical switches,<sup>[11]</sup> and lasers.<sup>[12,13]</sup> Among them, CdS-based PDs as the mainstay of optoelectronic devices are usually limited to the UV and visible light detection due to the constraint of light absorption ability with relatively slow response speed (> tens of milliseconds in most cases).<sup>[3]</sup> Nowadays, PDs with broadband response, fast speed, high sensitivity, and excellent stability are highly demanded.<sup>[14–17]</sup> Therefore, by combining with another semiconductor which possesses lower bandgap, it would extend the response spectra to longer wavelength. Moreover, an external bias voltage is usually necessary to operate PD devices for achieving fast detection speed and high photoresponsivity, which limits their applications in various environments.<sup>[18,19]</sup> Therefore, it is necessary and important to explore self-powered PDs based on CdS with broadband response, fast speed, and relatively high sensitivity.

As a pyroelectric material due to its noncentrosymmetry, wurtzite structured CdS crystal would generate an instantaneous potential from the induced pyroelectric polarization charges (pyrocharges) at two polar ends when heated or cooled.<sup>[20–23]</sup> Therefore, an increase

As one of the most studied semiconductors with wurtzite structure, cadmium sulfide (CdS) with a direct intermediate bandgap ( $\approx 2.42$  eV) exhibits a wide range of applications

CdS crystal would generate an instantaneous potential from the induced pyroelectric polarization charges (pyrocharges) at two polar ends when heated or cooled.<sup>[20–23]</sup> Therefore, an increase

Dr. Y. Dai, Dr. X. Wang, Dr. W. Peng, Dr. C. Xu, C. Wu, K. Dong, R. Liu, Prof. Z. L. Wang

School of Materials Science and Engineering  
Georgia Institute of Technology  
Atlanta, GA 30332-0245, USA  
E-mail: zhong.wang@mse.gatech.edu

Dr. Y. Dai  
Key Laboratory of Advanced Ceramics and Machining Technology  
Ministry of Education  
School of Materials Science and Engineering  
Tianjin University  
Tianjin 300072, China

Dr. W. Peng  
School of Electronic and Information Engineering  
Xi'an Jiaotong University  
Xi'an 710049, China

Prof. Z. L. Wang  
Beijing Institute of Nanoenergy and Nanosystems  
Chinese Academy of Sciences  
Beijing 100083, China



The ORCID identification number(s) for the author(s) of this article can be found under <https://doi.org/10.1002/adma.201705893>.

DOI: 10.1002/adma.201705893

in temperature for CdS nanowire (NW) caused by light illumination would result in a distribution of the pyroelectric potential along the polar direction of CdS NW. By forming a pn junction between p-type semiconductor and n-CdS,<sup>[24]</sup> the light-induced pyroelectric potential will modulate the built-in electric field of the pn junction, and thus modify the optoelectronic processes of charge carriers, which is referred to as the pyro-phototronic effect,<sup>[25–27]</sup> a three-way coupling effect among pyroelectricity, photoexcitation, and semiconductor. The pyro-phototronic effect could be utilized to achieve fast speed and broadband photosensing performances.

Here, a self-powered flexible PD has been fabricated based on p-Si/n-CdS NWs heterostructure by a simple hydrothermal synthesis. This self-powered PD shows a broadband response range, even beyond the limitation of the intrinsic bandgap of Si and CdS,<sup>[28]</sup> from UV (325 nm) to near infrared (NIR) (1550 nm) under zero bias with fast response speed, which is attributed to the pyro-phototronic effect. The light-induced pyroelectric potential is utilized to modulate the optoelectronic processes of charge carriers and thus improve the photoresponse performance. Upon 325 nm laser illumination, the rise time and fall time of the self-powered flexible PD are 245 and 277  $\mu\text{s}$ , respectively. Meanwhile, the photoresponsivity  $R$  and specific detectivity  $D^*$  are both enhanced by 67.8 times regarding to the relative peak-to-peak current, compared with those only based on the photovoltaic effect-induced photocurrent. Upon 1060 nm laser illumination, the response speed of the self-powered flexible PD is 492  $\mu\text{s}$  for the rise time and 654  $\mu\text{s}$  for the fall time. The photoresponsivity  $R$  and specific detectivity  $D^*$  are both improved with the enhancement of 17.4 times. The working mechanisms corresponding to different laser illuminations are carefully investigated. This Si/CdS self-powered flexible PD device is compatible with the traditional integrated circuit technology and thus would find extensive applications in various environments, such as wearable sensors, optothermal detections, ultrafast optics, optical communications, and health monitoring. This work not only provides an in-depth understanding of the pyro-phototronic effect on the pn junction heterostructure, but also offers a novel way to design and develop fast speed, stable, and broadband response self-powered flexible PDs.

The schematic structure of the self-powered p-Si/n-CdS heterostructure flexible PD is illustrated in **Figure 1a**. First, a p-type (100) Si wafer with a thickness of 0.5 mm was etched to dozens of micrometers in thickness in alkaline solution with high concentration (30 wt% KOH) in order to reduce the carrier transport time and achieve good flexibility (top left panel of **Figure 1b**). The flexible Si wafer was further etched into many micropylamids with a bottom edge length of 3–7  $\mu\text{m}$  on its surface in 5 wt% KOH solution in order to enhance the light absorption efficiency, as shown in **Figure 1b** (bottom left panel). Then, a CdS NW array was perpendicularly grown on the surfaces of Si micropylamids through a hydrothermal synthesis to form the p-Si/n-CdS heterojunction. The top-view and side-view (top right panel and bottom right panel of **Figure 1b**, and **Figure S1a,b**, Supporting Information) scanning electron microscopy (SEM) images indicate CdS NWs with an average length of 600 nm and an average diameter of 50 nm. Single-crystalline wurtzite structure and polar  $c$ -axis growth direction of the as-grown CdS NWs were further confirmed

by high-resolution transmission electron microscopy image (**Figure S1c**, Supporting Information) and corresponding select area electron diffraction pattern (**Figure S1d**, Supporting Information). Finally, indium-tin oxide (ITO) and aluminum (Al) were deposited on the n-CdS NW array as the transparent top-electrode and the p-type Si substrate as bottom-electrode, respectively. Detailed fabrication process is described in the Experimental Section.

Corresponding energy levels of the materials utilized to form the self-powered p-Si/n-CdS flexible PD are presented in **Figure 1c**. The valence band (VB) and conduction band (CB) of the silicon and CdS are  $-5.17$  and  $-6.82$  eV,  $-4.05$  and  $-4.40$  eV, versus vacuum, respectively.<sup>[29,30]</sup> Upon laser illumination, photogenerated carries are generated at the interface between Si and CdS, separated by the built-in electric field ( $E_{\text{built-in}}$ ) derived from the pn junction, and finally collected by the two electrodes, forming the photocurrent. The current–voltage ( $I$ – $V$ ) characteristics of the self-powered p-Si/n-CdS PD under 325, 442, 1060, and 1550 nm laser illumination are measured and plotted in **Figure 1d** and **Figure S2** (Supporting Information). Upon 325 nm, 442 and 1060 nm laser illuminations, the p-Si/n-CdS PD shows photoresponse behavior at a 2 V forward bias. The output current increases gradually from 30.4 to 69.5  $\mu\text{A}$  with an increasing power density from 0 to 4  $\text{mW cm}^{-2}$  under 1060 nm laser illumination at a 2 V forward bias. However, upon 1550 nm laser illumination, the p-Si/n-CdS PD shows no photoresponse due to the bandgap limitation of Si and CdS, even under large power density illumination ( $10 \text{ mW cm}^{-2}$ ).

When the laser is irradiated on the self-powered p-Si/n-CdS flexible PD with a rapid rise in temperature, the pyrocharges would be generated at both ends of a CdS NW due to the pyroelectric effect. The negative pyrocharges are created at the  $-c$  end of CdS NW under laser illumination and simultaneously the positive pyrocharges are created at the  $+c$  end of CdS NW, as shown in **Figure 1e** (top panel). Therefore, a pyroelectric electric field ( $E_{\text{pyro}}$ ) along the CdS NW would be achieved, which is equivalent to a potential applied on the self-powered PD. The time-dependent change of the  $E_{\text{pyro}}$  (or pyrocharges) inside the CdS NW can effectively drive the flow of electrons through external circuits and generate the pyroelectric current. The pyroelectric current can be expressed as  $I_{\text{pyro}} = AP_c(dT/dt)$ , where  $A$  is the electrode area and  $P_c$  is the pyroelectric coefficient, and the  $I_{\text{pyro}}$  is proportional to  $dT/dt$ . Therefore, any change in temperature will produce pyrocharges, and the temperature-change rate  $dT/dt$  determines the intensity of the pyroelectric current.<sup>[25,31–33]</sup> When the  $E_{\text{pyro}}$  is consistent with the  $E_{\text{built-in}}$  and thus would enhance the instantaneous short-circuit current (**Figure 1f**). On the contrary, when the laser illumination is turned off suddenly, a rapid decrease in temperature happens within CdS NW, giving rise to the opposite pyrocharge distribution at the two ends of the CdS NW (bottom panel in **Figure 1e**). At this time, the direction of the  $E_{\text{pyro}}$  is opposite to that of the  $E_{\text{built-in}}$ . Therefore, reversed output currents are obtained instantaneously (**Figure 1f**).

Based on the pyro-phototronic effect in CdS, a four-stage photoresponse behavior upon 1060 nm laser illumination without external bias voltage for the p-Si/n-CdS flexible PD is observed in **Figure 1f**, and an enlarged four-stage photoresponse

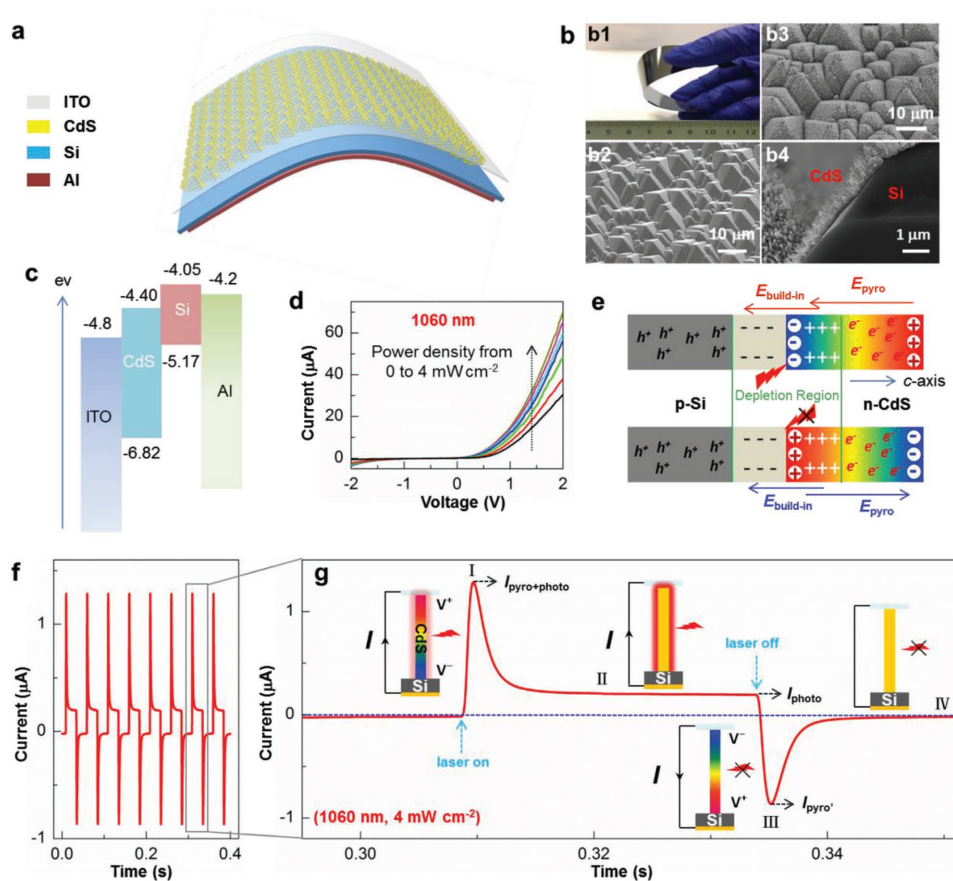


**Figure 1.** Structure, characterization, and working mechanism of the self-powered p-Si/n-CdS heterostructure flexible PD. a) Schematic structure of the self-powered PD. b) Characterizations of the self-powered PD, (b1) an optical image of the etched Si wafer with good flexibility, (b2) SEM image of the etched Si wafer surface, (b3,b4) top view (b3) and side view (b4) of the CdS NW array synthesized on the etched Si wafer. c) Energy band diagram of the self-powered PD. Energies are expressed in electron volts, using the electron energy in vacuum as a reference. d)  $I$ - $V$  characteristics under 1060 nm illumination with different power densities from 0 to  $4 \text{ mW cm}^{-2}$  when a 2 V bias is applied for the pn junction PD. e) Schematic potential distribution of p-Si/n-CdS heterojunction as turning on (top panel) and turning off (bottom panel) laser to illustrate the working mechanism of the pyro-phototronic effect. f) Photoresponse behavior of the self-powered PD under 1060 nm laser illumination with the power density of  $4 \text{ mW cm}^{-2}$  under zero bias. g) An enlarged view taken from the marked areas in (f), displaying a typical four-stage photoresponse behavior. The insets in (g) are schematic illustrations of the fundamental working mechanism of the pyro-phototronic effect corresponding to different stages, indicating the corresponding schematic circuit diagram with pyroelectric potential and light-induced heating effect in CdS NW.

dynamic behavior is presented in Figure 1g. In order to present our results more clearly, we define the photocurrent as positive. For the first stage, due to an instantaneous temperature rise within CdS NWs under laser illumination, a sharp current peak is induced by the pyro-phototronic effect ( $dT/dt > 0$ ). The corresponding maximum output current is called as  $I_{\text{pyro+photo}}$ , where the subscript “pyro+photo” indicates that the instantaneous output current is from the pyroelectric effect and photovoltaic effect. For the second stage, the output current is drastically reduced due to the disappearance of the pyroelectric current without temperature variation ( $dT/dt = 0$ ) and returns to a steady value called as  $I_{\text{photo}}$ , where the subscript “photo” indicates that the output current is from the photocurrent caused by the photovoltaic effect only. For the third stage, the laser illumination is turned off and a reversed peak in output current ( $I_{\text{pyro}}$ ) was formed due to the reversed pyrocharge distribution by instantaneous temperature decrease ( $dT/dt < 0$ ). For the fourth stage, the output current (dark current) restores

to a stable value near zero accompanied by the disappearance of the pyroelectric current ( $dT/dt = 0$ ), because the temperature of CdS NW returns to room temperature without the laser illumination. In addition, the piezo-phototronic effect derived from CdS NWs would be induced and change the photoresponse performance of this p-Si/n-CdS flexible heterojunction PD when under deformation.<sup>[7]</sup> If the piezocharges produced by externally applied strain and the pyrocharges produced by laser illumination are both negative (or both positive) at the interface, the strain would strengthen the effective pyropotential and thus enhance the pyro-phototronic effect-induced photocurrent  $I_{\text{pyro+photo}}$ , otherwise it would weaken the  $I_{\text{pyro+photo}}$ .<sup>[27]</sup> The four-stage photoresponse behaviors of the self-powered p-Si/n-CdS flexible PD under 325, 442, 1060, and 1550 nm laser illuminations at zero bias voltage are shown in Figure 2a, presenting broadband response from UV to NIR wavelength. For the 325, 442, and 1060 nm wavelengths, the four-stage photoresponse behavior shows larger  $I_{\text{pyro+photo}}$  ( $> 0.9 \mu\text{A}$ ) than

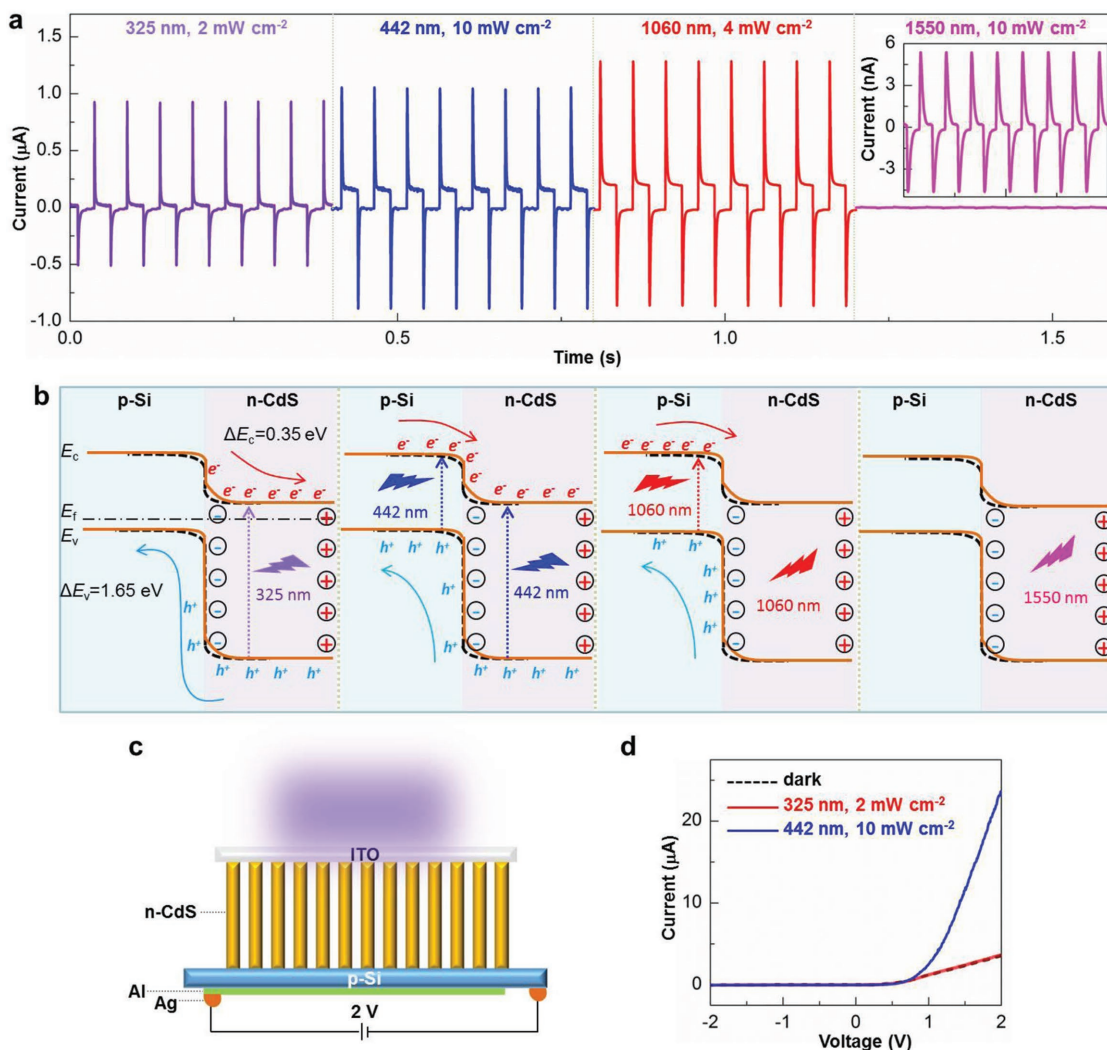


**Figure 2.** Broadband response of the self-powered p-Si/n-CdS heterostructure flexible PD. a) Photoresponse behaviors of the self-powered PD under 325, 442, 1060, and 1550 nm laser illuminations at 0 V bias voltage. The inset is the enlarged photoresponse for 1550 nm laser illumination. b) Schematic energy band diagrams of the p-Si/n-CdS heterojunction without (black dotted line) and with (orange line) 325, 442, 1060, and 1550 nm laser illuminations, illustrating different working mechanisms based on the pyro-phototronic effect. c) Schematic diagram of experimental setup for the photoresponse measurement of the Si substrate. d) *I*–*V* characteristics of the Si substrate under dark condition, 325 nm (2 mW cm<sup>-2</sup>) and 442 nm (10 mW cm<sup>-2</sup>) laser illuminations when applying a 2 V bias.

that ( $\approx 4.6$  nA) of the 1550 nm wavelength due to the existence of photogenerated carriers. It is worth noting that lasers with different wavelengths have different effects on the self-powered p-Si/n-CdS flexible PDs, and the different working mechanisms are schematically illustrated in Figure 2b. When the laser is irradiated on the self-powered PD, an instantaneous temperature rise in the CdS NWs leads to the negative pyrocharges distributed at the local interface of the pn junction as shown in Figure 1e, which would attract the holes in the p-type Si moving toward and repel the electrons in the n-type CdS away from the interface of p-Si/n-CdS heterojunction, leading to an upward bending of the energy band (orange line in Figure 2b) for both Si and CdS based on Anderson's model.<sup>[34]</sup> For 325 nm laser illumination, the UV photons are mainly absorbed by the CdS NWs, and the photogenerated electrons and holes in the CdS NWs are separated and collected by the ITO and Al electrodes,

respectively, generating  $I_{\text{photo}}$ , as shown in Figure 2a for 325 nm. Moreover, the pyroelectric potential and upward bending of the energy band facilitate the transport of charge carriers, and thus an instantaneous high output current is obtained. For 442 nm laser illumination, the visible photons are absorbed by both of Si substrate and CdS NWs, producing a much larger  $I_{\text{photo}}$  compared to that of 325 nm laser illumination, as shown in Figure 2a for 442 nm. Therefore, it is concluded that the  $I_{\text{photo}}$  is mainly from the photogenerated carriers of p-Si, which is also confirmed by measuring the photoresponse of the Si substrate alone. As schematically shown in Figure 2c, the Si substrate of the self-powered PD was connected with two Ag electrodes and the laser was irradiated from the side of the CdS NWs. *I*–*V* characteristics of the Si substrate under dark condition, 325 and 442 nm laser illuminations are presented in Figure 2d, respectively, indicating that the photoresponse of the Si substrate

under 442 nm laser illumination is much larger than that under 325 nm laser illumination. Similarly, for 1060 nm laser illumination, the larger  $I_{\text{photo}}$  is obtained because the NIR photons are mainly absorbed by the Si substrate, according to the transmission spectrum of CdS NW array as shown in Figure S3 (Supporting Information). For 1550 nm laser illumination, since this wavelength goes beyond the absorption range of Si and CdS, it could not produce photogenerated carriers, as shown in Figure 2b for 1550 nm. However, the pyroelectric effect could still lead to the generation of pyrocharges, form the  $E_{\text{pyro}}$ , and thus achieve an instantaneous rise or drop in the output current. The temperature change of CdS under 1550 nm laser illumination with the power density of  $10 \text{ mW cm}^{-2}$  is calculated and presented in Note S1 and Figure S4 (Supporting Information).

The photoresponse of the self-powered p-Si/n-CdS heterojunction flexible PD under 1060 nm laser illumination with different power densities from  $0.32$  to  $4.0 \text{ mW cm}^{-2}$  at zero bias voltage is measured and summarized systematically in Figure 3a. Obviously, the four-stage dynamic behavior is observed for all power densities, showing good pyro-phototronic effect. The  $I_{\text{pyro+photo}}$ ,  $I_{\text{photo}}$ , and the relative peak-to-peak ( $I_{\text{pyro+photo}} - I_{\text{pyro}}$ ) under each power density are derived from Figure 3a and plotted in Figure 3b. These currents increase with the power density of laser illumination, and the maximum enhancement factor for  $(I_{\text{pyro+photo}} - I_{\text{pyro}})/I_{\text{photo}}$  and  $I_{\text{pyro+photo}}/I_{\text{photo}}$  are 17.9 and 8.8 at the power density of  $0.72 \text{ mW cm}^{-2}$ , respectively.

As critical parameters of PDs, the corresponding photoresponsivity  $R$  and specific detectivity  $D^*$  under each power density are further calculated and summarized in Figures 3c and Figure S5 (Supporting Information).  $R$  is defined as  $R = \frac{\Delta I}{P_{\text{ill}}}$ ,

where  $P_{\text{ill}} = I_{\text{ill}} \times S$  is the illumination power on the PD,  $I_{\text{ill}}$  is the power density,  $S$  is the effective area ( $16 \text{ mm}^2$ ) of the PD, and  $\Delta I$  is photocurrent.  $D^*$  is calculated as  $D^* = \frac{R}{\sqrt{2qI_{\text{dark}}/S}}$

by considering the dark current as the major noise, where  $q$  is the electronic charge, and  $I_{\text{dark}}$  is the dark current, which is about  $10^{-11} \text{ A}$  (Figure S6, Supporting Information).<sup>[35,36]</sup> For all power densities, the photoresponsivity  $R$  is enhanced greatly via the pyro-phototronic effect. For photocurrent  $I_{\text{photo}}$ , the maximum  $R$  of  $0.34 \text{ mA W}^{-1}$  is obtained under 1060 nm laser illumination with the power density of  $1.1 \text{ mW cm}^{-2}$ . For the relative peak-to-peak current ( $I_{\text{pyro+photo}} - I_{\text{pyro}}$ ) and the  $I_{\text{pyro+photo}}$ , the maximum  $R$  value reaches 5.9 and  $3.1 \text{ mA W}^{-1}$  at the power density of  $1.1 \text{ mW cm}^{-2}$ , with the enhancement of 17.4 times and 9.1 times by the pyro-phototronic effect, respectively. The maximum detectivity  $D^*$  value also reaches as high as  $1.3 \times 10^{12}$  Jones according to the relative peak-to-peak current ( $I_{\text{pyro+photo}} - I_{\text{pyro}}$ ) and  $6.9 \times 10^{11}$  Jones according to the  $I_{\text{pyro+photo}}$  at the power density of  $1.1 \text{ mW cm}^{-2}$  due to the low dark current. Moreover, the rise time and fall time of the self-powered PD as a function of the power density were calculated and summarized in Figure 3d. With the increase of power

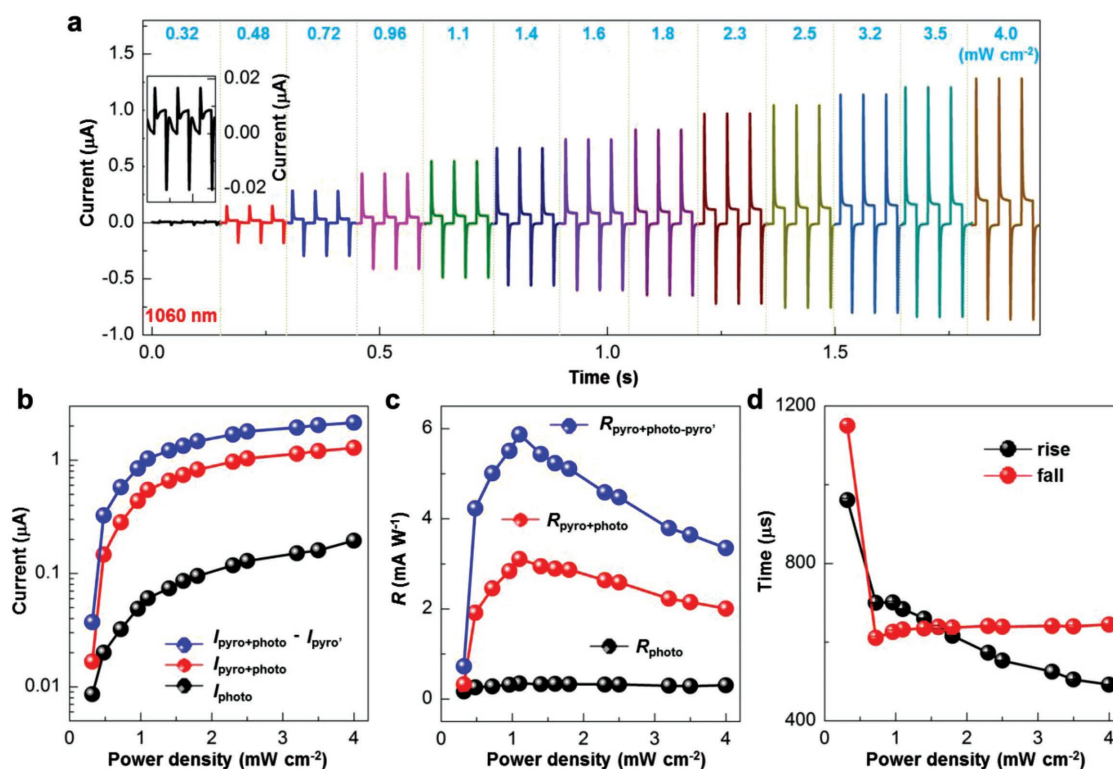


**Figure 3.** Pyro-phototronic effect on the self-powered p-Si/n-CdS heterojunction flexible PD under 1060 nm laser illumination. a)  $I-t$  characteristics of the self-powered PD with different power densities from  $0.32$  to  $4.0 \text{ mW cm}^{-2}$ . Inset: Enlarged  $I-t$  characteristics with a  $0.32 \text{ mW cm}^{-2}$  power density. b)  $I_{\text{pyro+photo}}$ ,  $I_{\text{photo}}$ , and  $I_{\text{pyro+photo}} - I_{\text{pyro}}$  of the self-powered PD as a function of the power density. c) Corresponding  $R_{\text{pyro+photo}}$ ,  $R_{\text{photo}}$ , and  $R_{\text{pyro+photo-pyro}}$  of the self-powered PD as a function of the power density. d) Corresponding rise time and fall time of the self-powered PD as a function of the power density.

density from 0.32 to 4.0 mW cm<sup>-2</sup>, the rise time (defined as the time taken for the current increasing from 10% to 90% of maximum photocurrent) decreases from 961 to 492 μs and fall time (defined as the time taken for the current decreasing from 90% to 10% of maximum photocurrent) decreases from 1150 to 645 μs, which correspond to a 48.8% and 43.9% reduction, respectively. As we mentioned above, the  $I_{\text{pyro}}$  is proportional to  $dT/dt$ . Therefore, the greater the incident power density, the faster the temperature-change rate ( $dT/dt$ ), inducing larger  $I_{\text{pyro}}$  and faster response speed. These results indicate that the laser illumination with larger power density is more conducive to the pyro-phototronic effect and thus achieves faster response speed, indicating a novel approach to develop fast response PDs for strong light detections based on the pyro-phototronic effect.

Similar results for 325, 442, and 1550 nm laser illumination are shown in Figures S7–S10 in the Supporting Information, respectively. For 325 nm laser illumination with the power density of 1.2 mW cm<sup>-2</sup>, the maximum  $R_{\text{pyro+photo-pyro'}}$  of 4.6 mA W<sup>-1</sup> and the maximum  $R_{\text{pyro+photo}}$  of 2.8 mA W<sup>-1</sup> could be obtained, which is about 67.8 times and 41.5 times of  $R_{\text{photo}}$ . The maximum value of  $D^*$  is obtained as  $1.0 \times 10^{12}$  Jones for  $D_{\text{pyro+photo-pyro'}}$  and  $6.2 \times 10^{11}$  Jones for  $D_{\text{pyro+photo}}$ . The rise time and fall time at the power density of 2 mW cm<sup>-2</sup> are 245 and 277 μs, respectively, which are faster than those of most previously reported CdS-based and other nanostructure PDs.<sup>[3,6,7,37–44]</sup> For 442 nm laser illumination with the power density of 0.23 mW cm<sup>-2</sup>, the maximum  $R_{\text{pyro+photo-pyro'}}$  of 4.1 mA W<sup>-1</sup> and the maximum  $R_{\text{pyro+photo}}$  of 1.8 mA W<sup>-1</sup> could be obtained, which is about 60.2 times and 25.9 times of  $R_{\text{photo}}$ . The maximum value of  $D^*$  is obtained as  $9.2 \times 10^{11}$  Jones for  $D_{\text{pyro+photo-pyro'}}$  and  $4.0 \times 10^{11}$  Jones for  $D_{\text{pyro+photo}}$ . The rise time and fall time at the power density of 10 mW cm<sup>-2</sup> are 368 and 440 μs, respectively. For 1550 nm laser illumination with the power density of 10 mW cm<sup>-2</sup>, the maximum  $R_{\text{pyro+photo-pyro'}}$  of 6.2 μA W<sup>-1</sup> and the maximum  $R_{\text{pyro+photo}}$  of 2.9 μA W<sup>-1</sup> could be obtained. The maximum value of  $D^*$  is obtained as  $1.4 \times 10^9$  Jones for  $D_{\text{pyro+photo-pyro'}}$  and  $6.4 \times 10^8$  Jones for  $D_{\text{pyro+photo}}$ . The rise time and fall time at the power density of 10 mW cm<sup>-2</sup> are 1.47 and 1.37 ms, respectively. In addition, the photoresponsivity  $R_{\text{pyro+photo}}$  of the self-powered p-Si/n-CdS PD as a function of laser wavelength from 325 to 1550 nm based on the pyro-phototronic effect is presented in Figure S11 (Supporting Information), further confirming a broad spectral response from UV to NIR. These results indicate that the photoresponse performance of the self-powered flexible PD could be greatly improved by the pyro-phototronic effect in a broad spectral region.

The frequency dependence of the self-powered flexible PD under 1060 nm laser illumination with the power density of 4.0 mW cm<sup>-2</sup> is investigated and the corresponding  $I$ - $t$  characteristics are presented in Figure 4a and Figure S12 (Supporting Information). The optical chopper frequency varies from 2 to 20 Hz in Figure 4a. It is clear that the  $I_{\text{photo}}$  does not change with the varying frequency, but the  $I_{\text{pyro+photo}}$  is slightly reduced at lower frequency. The rise time and fall time are extracted from Figure 4a and plotted in Figure 4b. The rise time decreases from 2230 to 492 μs, and the fall time decreases from 2860 to 645 μs with the frequency increasing from 2 to 20 Hz. Since the laser on or off on the PD device is controlled by an optical

chopper's rotation with a certain frequency and the laser spot has a certain area, the time it takes for the laser spot to illuminate the PD device would be shorter at higher frequency. Therefore, due to the enhanced temperature-change rate ( $dT/dt$ ) under higher frequency, the  $I_{\text{pyro}}$  and response speed would increase with an increase in frequency (in a certain range). This result indicates that in a certain range the higher frequency is more beneficial to the pyro-phototronic effect.

In addition, the bias voltage effect on the pyro-phototronic effect is carefully investigated under different bias voltages from 0.01 to 2.0 V when applying 1060 nm illumination with the power density of 4 mW cm<sup>-2</sup> at 20 Hz, as presented in Figure 4c. When the forward bias voltage is smaller than 1.4 V, the photoresponse presents obvious four-stage dynamic behavior in each cycle, clearly showing the pyro-phototronic effect on CdS NWs. With the increasing of bias voltage, the photocurrent and dark current increase, whereas the  $I_{\text{pyro+photo}}$  and  $I_{\text{pyro'}}$  gradually decrease until disappear when the bias voltage is more than 1.0 V. The enhancement factor  $E$  ( $= I_{\text{pyro+photo}}/I_{\text{photo}}$ ) decreases with the increasing bias voltage and a maximum value of 7.4 could be obtained at zero bias voltage as shown in Figure 4d, indicating that the joule heat caused by the applied bias voltage would weaken the pyro-phototronic effect. Meanwhile, the response speed also decreases with increasing bias voltage due to the weakened pyro-phototronic effect. Moreover,  $I$ - $t$  characteristics of the self-powered PD at a reverse bias voltage of -0.8 V at the power density of 4 mW cm<sup>-2</sup> are shown in Figure S13 (Supporting Information), presenting the typical pyro-phototronic effect-induced four-stage dynamic behavior. However, since the direction of the pyroelectric potential is opposite to that of the applied bias voltage, when turning on or off the laser illumination, the instantaneous current peaks indicated in Figure S13 (Supporting Information) are opposite to the directions of the stable currents, further confirming the working mechanism of the pyro-phototronic effect we mentioned above in Figure 1e. These results indicate that the pyro-phototronic effect is controllable by the external conditions, such as illumination frequency and applied bias voltage. Furthermore, similar results are obtained for 325, 442, and 1550 nm laser illumination shown in Figures S14–S16 in the Supporting Information, respectively.

In summary, the light-induced pyro-phototronic effect has been utilized as an effective approach to enhance the photoresponse performance in a broadband range. A self-powered flexible PD based on p-Si/n-CdS NWs heterostructure has been fabricated and shows a broadband response from UV (325 nm) to NIR (1550 nm) under zero bias with fast response speed, which is even beyond the bandgap limitation of Si and CdS. This phenomenon could be attributed to the pyro-phototronic effect of CdS due to the light-induced heating/cooling. The light-induced pyroelectric potential is utilized to modulate the optoelectronic processes and thus improve the photoresponse performance. The working mechanisms corresponding to different laser illuminations are investigated carefully. In addition, the influences of illumination frequency and applied bias voltage on the pyro-phototronic effect are studied as well. This Si/CdS self-powered flexible PD device is compatible with the traditional integrated circuit technology and thus would find extensive applications

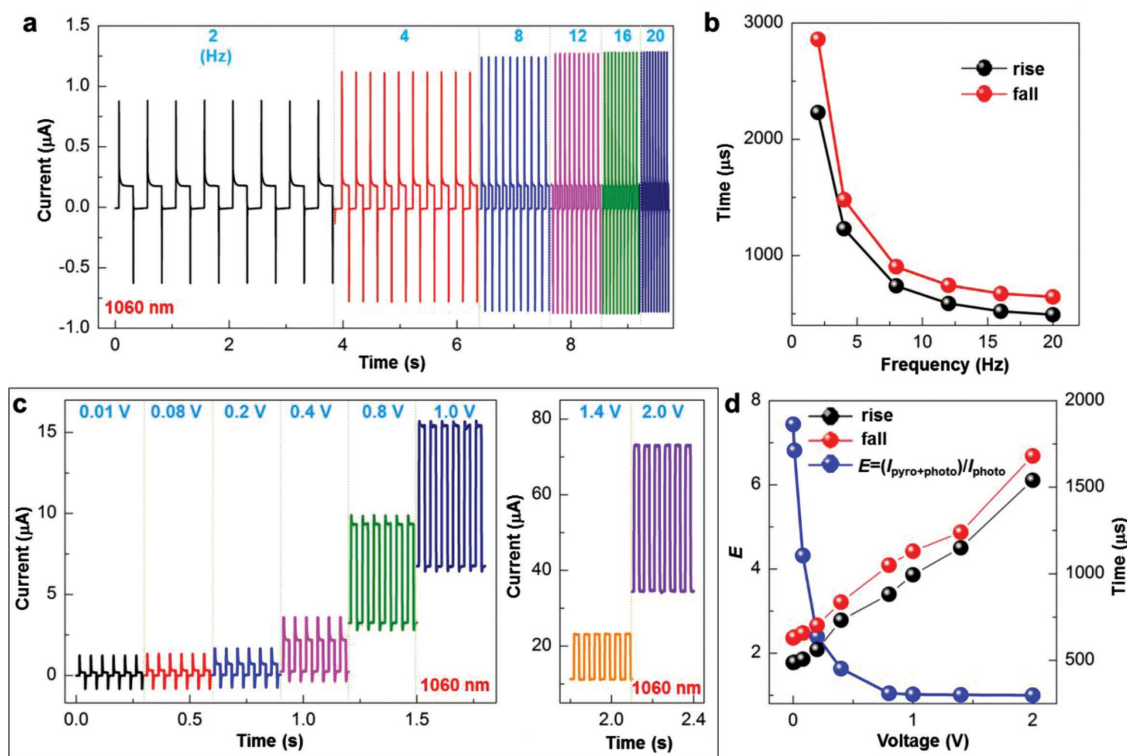


**Figure 4.** Impacts of frequency and bias voltage on the pyro-phototronic effect under 1060 nm laser illumination. a)  $I-t$  characteristics of the self-powered PD at different frequencies from 2 to 20 Hz (power density  $\approx 4 \text{ mW cm}^{-2}$ ). b) Corresponding rise time and fall time of the self-powered PD as a function of frequency. c)  $I-t$  characteristics of the self-powered PD at different bias voltages from 0.01 to 2.0 V (power density  $\approx 4 \text{ mW cm}^{-2}$ ) under 20 Hz. d) Corresponding rise time, fall time, and enhancement factor  $E (= I_{\text{pyro+photo}}/I_{\text{photo}})$  of the self-powered PD as a function of bias voltage.

in various environments. This work not only provides an in-depth understanding of the pyro-phototronic effect on the pn junction heterostructure, but also offers a novel and effective way to design and develop fast speed, stable, and broadband response self-powered PDs.

## Experimental Section

**Fabrication Process of the p-Si/n-CdS Flexible PD:** The p-type silicon wafer (1–10 Ω cm, B-doped (100) wafer, Universal Wafer) was etched to dozens of micrometers in thickness in 30 wt% KOH solution at 80 °C, and then was further etched into many micropylramids on the surface by 5 wt% KOH with 5 vol% isopropanol at 80 °C for 45 min. After then, the etched Si wafer with micropylramids was ultrasonically cleaned in acetone, deionized water, and alcohol for 3 min, respectively. Next, the etched flexible Si wafer with the growth surface facing down was placed into a 90 mL autoclave with a mixture nutrient solution including  $9 \times 10^{-3}$  M glutathione,  $15 \times 10^{-3}$  M thiourea, and  $15 \times 10^{-3}$  M cadmium nitrate. The autoclave was placed into an oven at 200 °C for 8 h for the growth of CdS, and the obtained sample was cleaned with distilled water and vacuum-dried at 70 °C. Finally, the top electrode (ITO) on CdS NWs and bottom electrode (Al) on Si substrate was deposited by RF magnetron sputtering (PVD75 System, Kurt. J. Lesker Co.) under the condition of the chamber pressure of 8 mTorr and power of 100 W for 30 min, respectively. Testing wires were connected to the top ITO and bottom Al electrodes using silver paste.

**Characterization and Measurement:** Detailed microscopic structures of the micropyramid structure of Si and CdS NWs were characterized by SEM (Hitachi SU8010). A transmission spectrum of CdS NWs was characterized using an UV-vis spectrophotometer (JASCO V-630).  $I-V$

and  $I-t$  characteristics of the self-powered PDs were measured by using a computer-controlled measurement system with a Stanford SRS low noise current preamplifier (SR570)/SRS low noise voltage preamplifier (SR560) in conjunction with a GPIB controller (GPIB-USB-HS, NI 488.2). The optical input stimuli were provided by a He-Cd dual-color laser (325 and 442 nm) (Model No. KI57511-G, Kimmon Koha Co., Ltd.) and fiber coupled laser sources (1060 and 1550 nm) (MCLS1, Thorlabs Inc.) whose light power density can be adjusted by a continuously variable filter and measured by a thermopile powermeter (Newport Model 1919-R).

## Supporting Information

Supporting Information is available from the Wiley Online Library or from the author.

## Acknowledgements

Y.J.D., X.F.W., and W.B.P. contributed equally to this work. Research was supported by U.S. Department of Energy, Office of Basic Energy Sciences (Award DE-FG02-07ER46394) (the piezotronic and piezophototronic device fabrication and measurements), and the National Science Foundation (DMR-1505319) (materials synthesis and application in sensors).

## Conflict of Interest

The authors declare no conflict of interest.

## Keywords

broadband, CdS nanowires, photosensing, pyro-phototronic effect, self-powered

Received: October 10, 2017

Revised: November 20, 2017

Published online:

- [1] J. Cai, J. Jie, P. Jiang, D. Wu, C. Xie, C. Wu, Z. Wang, Y. Yu, L. Wang, X. Zhang, Q. Peng, Y. Jiang, *Phys. Chem. Chem. Phys.* **2011**, *13*, 14663.
- [2] O. Hayden, A. B. Greytak, D. C. Bell, *Adv. Mater.* **2005**, *17*, 701.
- [3] K. Deng, L. Li, *Adv. Mater.* **2014**, *26*, 2619.
- [4] D. Zheng, H. Fang, P. Wang, W. Luo, F. Gong, J. C. Ho, X. Chen, W. Lu, L. Liao, J. Wang, W. Hu, *Adv. Funct. Mater.* **2016**, *26*, 7690.
- [5] L. Li, P. Wu, X. Fang, T. Zhai, L. Dai, M. Liao, Y. Koide, H. Wang, Y. Bando, D. Golberg, *Adv. Mater.* **2010**, *22*, 3161.
- [6] P. Guo, W. Hu, Q. Zhang, X. Zhuang, X. Zhu, H. Zhou, Z. Shan, J. Xu, A. Pan, *Adv. Mater.* **2014**, *26*, 2844.
- [7] Y. Dai, X. Wang, W. Peng, H. Zou, R. Yu, Y. Ding, C. Wu, Z. L. Wang, *ACS Nano* **2017**, *11*, 7118.
- [8] Z. Fan, H. Razavi, J. W. Do, A. Moriwaki, O. Ergen, Y. L. Chueh, P. W. Leu, J. C. Ho, T. Takahashi, L. A. Reichertz, S. Neale, K. Yu, M. Wu, J. W. Ager, A. Javey, *Nat. Mater.* **2009**, *8*, 648.
- [9] L. Li, H. Lu, Z. Yang, L. Tong, Y. Bando, D. Golberg, *Adv. Mater.* **2013**, *25*, 1109.
- [10] J. Tang, Z. Huo, S. Brittman, H. Gao, P. Yang, *Nat. Nanotechnol.* **2011**, *6*, 568.
- [11] B. Piccione, C. H. Cho, L. K. Van Vugt, R. Agarwal, *Nat. Nanotechnol.* **2012**, *7*, 640.
- [12] A. Pan, W. Zhou, E. S. P. Leong, R. Liu, A. H. Chin, B. Zou, C. Z. Ning, *Nano Lett.* **2009**, *9*, 784.
- [13] X. Duan, Y. Huang, R. Agarwal, C. M. Lieber, *Nature* **2003**, *421*, 241.
- [14] T. Zhai, L. Li, X. Wang, X. Fang, Y. Bando, D. Golberg, *Adv. Funct. Mater.* **2010**, *20*, 4233.
- [15] T. Zhai, X. Fang, L. Li, Y. Bando, D. Golberg, *Nanoscale* **2010**, *2*, 168.
- [16] G. Konstantatos, E. H. Sargent, *Nat. Nanotechnol.* **2010**, *5*, 391.
- [17] S. K. Ray, A. K. Katiyar, A. K. Raychaudhuri, *Nanotechnology* **2017**, *28*, 092001.
- [18] X. Wang, P. Wang, J. Wang, W. Hu, X. Zhou, N. Guo, H. Huang, S. Sun, H. Shen, T. Lin, M. Tang, L. Liao, A. Jiang, J. Sun, X. Meng, X. Chen, W. Lu, J. Chu, *Adv. Mater.* **2015**, *27*, 6575.
- [19] P. Guo, J. Xu, K. Gong, X. Shen, Y. Lu, Y. Qiu, J. Xu, Z. Zou, C. Wang, H. Yan, Y. Luo, A. Pan, H. Zhang, J. C. Ho, K. M. Yu, *ACS Nano* **2016**, *10*, 8474.
- [20] A. K. Katiyar, S. Mukherjee, M. Zeeshan, S. K. Ray, A. K. Raychaudhuri, *ACS Appl. Mater. Interfaces* **2015**, *7*, 23445.
- [21] G. Heiland, H. Ibach, *Solid State Commun.* **1966**, *4*, 353.
- [22] Y. Yang, J. H. Jung, B. K. Yun, F. Zhang, K. C. Pradel, W. X. Guo, Z. L. Wang, *Adv. Mater.* **2012**, *24*, 5357.
- [23] C. C. Hsiao, S. Y. Yu, *Sensors* **2012**, *12*, 17007.
- [24] Y. V. Shaldin, S. Matyjasik, *Semiconductors* **2014**, *48*, 562.
- [25] Z. Wang, R. Yu, C. Pan, Z. Li, J. Yang, F. Yi, Z. L. Wang, *Nat. Commun.* **2015**, *6*, 8401.
- [26] Z. Wang, R. Yu, X. Wang, W. Wu, Z. L. Wang, *Adv. Mater.* **2016**, *28*, 6880.
- [27] W. Peng, X. Wang, R. Yu, Y. Dai, H. Zou, A. C. Wang, Y. He, Z. L. Wang, *Adv. Mater.* **2017**, *29*, 1606698.
- [28] S. Manna, S. Das, S. P. Mondal, R. Singha, S. K. Ray, *J. Phys. Chem. C* **2012**, *116*, 7126.
- [29] R. Bao, C. Wang, L. Dong, C. Shen, K. Zhao, C. Pan, *Nanoscale* **2016**, *8*, 8078.
- [30] Z. Wang, R. Yu, X. Wen, Y. Liu, C. Pan, W. Wu, Z. L. Wang, *ACS Nano* **2014**, *8*, 12866.
- [31] A. K. Batra, M. D. Aggarwal, *Pyroelectric Materials*, SPIE Press, Bellingham, WA, USA **2013**.
- [32] Y. Yang, W. Guo, K. C. Pradel, G. Zhu, Y. Zhou, Y. Zhang, Y. F. Hu, L. Lin, Z. L. Wang, *Nano Lett.* **2012**, *12*, 2833.
- [33] Y. Yang, S. Wang, Y. Zhang, Z. L. Wang, *Nano Lett.* **2012**, *12*, 6408.
- [34] S. M. Sze, *CC/Eng. Tech. Appl. Sci.* **1982**, *27*, 28.
- [35] X. Gong, M. Tong, Y. Xia, W. Cai, J. S. Moon, Y. Cao, G. Yu, C.-L. Shieh, B. Nilsoon, A. J. Heeger, *Science* **2009**, *325*, 1665.
- [36] R. D. Jansen-van Vuuren, A. Armin, A. K. Pandey, P. L. Burn, P. Meredith, *Adv. Mater.* **2016**, *28*, 4766.
- [37] T. Gao, Q. H. Li, T. H. Wang, *Appl. Phys. Lett.* **2005**, *86*, 173105.
- [38] T.-Y. Wei, C.-T. Huang, B. J. Hansen, Y.-F. Lin, L.-J. Chen, S.-Y. Lu, Z. L. Wang, *Appl. Phys. Lett.* **2010**, *96*, 013508.
- [39] K. Heo, H. Lee, Y. Park, J. Park, H.-J. Lim, D. Yoon, C. Lee, M. Kim, H. Cheong, J. Park, J. Jian, S. Hong, *J. Mater. Chem.* **2012**, *22*, 2173.
- [40] G. Li, Y. Jiang, Y. Zhang, X. Lan, T. Zhai, G.-C. Yi, *J. Mater. Chem. C* **2014**, *2*, 8252.
- [41] L. D. Li, Z. Lou, G. Z. Shen, *ACS Appl. Mater. Interfaces* **2015**, *7*, 23507.
- [42] Y. Pei, R. Pei, X. Liang, Y. Wang, L. Liu, H. Chen, J. Liang, *Sci. Rep.* **2016**, *6*, 21551.
- [43] G. Y. Gou, G. Z. Dai, C. Qian, Y. F. Liu, Y. Fu, Z. Y. Tian, Y. K. He, L. G. Kong, J. L. Yang, J. Sun, Y. L. Gao, *Nanoscale* **2016**, *8*, 14580.
- [44] A. Sarkar, A. K. Katiyar, S. Mukherjee, S. K. Ray, *J. Phys. D: Appl. Phys.* **2017**, *50*, 145104.